JVST A
Journal of Vacuum Science & Technology A

ARTICLE

avs.scitation.org/journal/jva

Hollow cathode plasma electron source for low temperature deposition of cobalt films by electron-enhanced atomic layer deposition

Cite as: J. Vac. Sci. Technol. A 39, 042403 (2021); doi: 10.1116/6.0001033
Submitted: 16 March 2021 · Accepted: 17 May 2021 ·
Published Online: 8 June 2021

Zachary C. Sobell,[1] Andrew S. Cavanagh,[1] David R. Boris,[2] Scott G. Walton,[2] and Steven M. George[1]

AFFILIATIONS

[1]Department of Chemistry, University of Colorado, Boulder, Colorado 80309-0215
[2]Naval Research Laboratory, 4555 Overlook Ave. SW, Washington, DC 20375

Note: This paper is part of the 2022 Special Topic Collection on Atomic Layer Deposition (ALD).

ABSTRACT

The development of a hollow cathode plasma electron source (HC-PES) facilitated the rapid nucleation and low temperature deposition of thin cobalt films using electron-enhanced atomic layer deposition (EE-ALD). The Co EE-ALD was performed near room temperature (30–60 °C) using sequential exposures of cobalt tricarbonyl nitrosyl and low energy (100–200 eV) electrons. Electron-stimulated desorption of CO and NO surface species creates open sites for precursor adsorption to facilitate the low temperature film growth. The HC-PES displayed high electron currents, rapid ALD cycling, and low susceptibility to chemical interference. Electron steering optics were also used to mitigate the effects of sputtering in the HC-PES. The high electron currents from the HC-PES yielded rapid nucleation of cobalt films in as few as four EE-ALD cycles with Co growth rates over 2 Å/cycle on areas >4 cm^2. In high aspect ratio structures, transmission electron microscopy and energy dispersive spectroscopy analyses revealed a 4:1 topographical selectivity in favor of horizontal compared with vertical surfaces. This selectivity was attributed to the directional electron flux from the HC-PES. This topographical area selective deposition suggests that Co EE-ALD may be successful in achieving bottom-up fill of trenches and vias.

I. INTRODUCTION

The use of low energy electrons can facilitate the growth of thin films of metals, dielectrics, and semiconductors through electron-enhanced atomic layer deposition (EE-ALD).[1–4] EE-ALD uses sequential exposure of precursors and low energy electrons to deposit thin films. The precursor molecule first adsorbs on the substrate. Subsequently, the low energy electrons desorb the ligands from the precursor via electron-stimulated desorption (ESD).[5,6] The process of ligand desorption leaves behind open sites for further precursor adsorption. Repeating the precursor and low energy electron sequential exposures produces the EE-ALD film growth.

Similar to the behavior during thermal ALD,[7] both the electron exposure and precursor dose should display self-limiting behavior during EE-ALD. For the precursor dose, saturation is defined as the formation of one complete layer of precursor on the substrate. For the electron exposure, saturation is defined as the removal of all ligands from the saturated surface. Repetition of the sequential precursor and electron exposures should lead to thin film growth with Angstrom-level precision.

Electron-enhanced thin film growth has been demonstrated previously for the deposition of elemental silicon.[3] Silicon was deposited using sequential surface reactions with disilane (Si_2H_6) and low energy electrons as the reactants. The proposed mechanism was dissociative adsorption of disilane on the surface and then the removal of hydrogen by ESD using low energy electrons. The removal of hydrogen from the surface leaves behind dangling bonds on the silicon, which are then available for subsequent disilane adsorption. Silicon growth rates were determined to be 0.3 Å/cycle at room temperature and an electron energy of 100 eV.[3]

EE-ALD has also been demonstrated for the growth of hexagonal boron nitride (BN).[4] The h-BN was grown using borazine ($B_3N_3H_6$) and low energy electrons. Borazine is an ideal molecule for BN EE-ALD for several reasons. Borazine has a high vapor pressure and the 1:1 B:N stoichiometry needed for BN growth. Borazine also contains hydrogen that has been shown to be labile

from surfaces under electron radiation.[3,8,9] The BN EE-ALD was shown to be crystalline and turbostratic by XRD and transmission electron microscopy (TEM), respectively.[4] The proposed growth mechanism was the adsorption of the borazine rings parallel to the surface. The low energy electrons then desorb hydrogen, which allows the borazine rings to bond together. This hypothesis was supported by the distinct layered appearance of the BN films by TEM.[4]

The EE-ALD investigations discussed above utilized low energy electrons generated from an electron gun source based on thermionic emission.[1–4] Such electron gun sources are typically limited to fairly low electron currents because of space charge limits defined by the Child–Langmuir law.[10,11] In addition, the hot filament electron emitter is susceptible to chemical attack and deposition from the chemical precursors and reactive carrier gases. The time required for the film growth is long because of the low electron flux. The processing times are further lengthened due to the pump and purge times needed to ensure minimal precursor reaction with the hot electron filament. A more chemically insensitive electron source would allow shorter pump and purge times, significantly decreasing the processing time.

Compared with electron guns based on hot filaments, hollow cathode plasma electron sources (HC-PES) are much more robust and produce higher currents.[12,13] These sources take advantage of the "hollow cathode effect," where electron confinement within a hollow cavity cathode leads to high plasma densities.[14] The plasma electrons can then be extracted from the hollow cathode plasma to yield high current electron beams. Numerous designs for the HC-PES have evolved over the last 30 years.[15–17] Many of these HC-PES designs conveniently operate at pressures of 10–500 mTorr.[18–22] These conditions are compatible with many material processing procedures.

Because of their high electron density and chemical insensitivity, hollow cathodes can be employed for many applications.[17,23] The sputtered ions and plasma species from hollow cathodes have been used previously for thin film deposition.[24] The extracted electrons from hollow cathode plasmas can also be utilized to generate low electron temperature plasmas capable of delivering very low energy ions to adjacent surfaces in a wide variety of gases.[25,26] Electron beam injection from hollow cathodes has also been utilized for electron-enhanced surface etching.[27] This paper will utilize the HC-PES as a source of low energy electrons for Co EE-ALD.

This paper begins with a description of the basic operating principles of the HC-PES. The design and operation of the HC-PES is then discussed including the auxiliary electron steering optics needed to bend the electron beam to eliminate any downstream contamination from the hollow cathode. The paper then explores the results for Co EE-ALD obtained using the HC-PES. A direct comparison between the HC-PES and the previously employed thermionic emission electron gun is also given for Co EE-ALD. Finally, an examination of Co EE-ALD in high aspect ratio structures is presented using TEM analysis.

II. HOLLOW CATHODE PLASMA ELECTRON SOURCE

A. Hollow cathode plasma operation

An illustration of the operation of a hollow cathode plasma is shown by the following steps in Fig. 1.[28] (1) The hollow cathode plasma starts with an initial ionization event inside the hollow cathode body. This ionization event creates an ion-electron pair. (2) The positive ion is accelerated toward the negatively biased walls of the hollow cathode and strikes the wall with kinetic energy commensurate with the applied cathode voltage, i.e., several hundred eVs in this work. (3) The resulting collision is energetic enough to liberate secondary electrons. (4) The electrons are repelled from the negatively biased walls, enter the bulk plasma, and become trapped between the walls.

The events in the hollow cathode continue as follows: (5) As the electrons oscillate within the hollow cathode cavity, they can

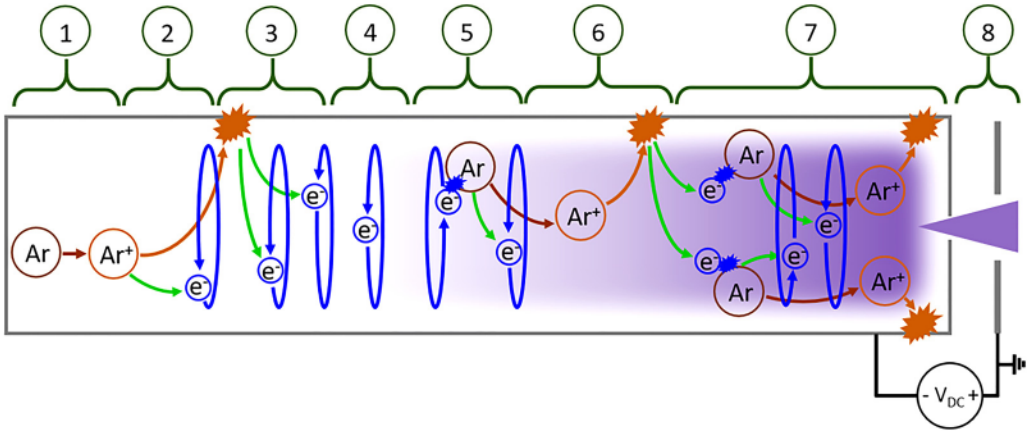

FIG. 1. Operation of hollow cathode plasma can be described as: (1) an initial ionization event; (2) ion accelerated to cathode wall; (3) ion impacts on cathode wall produce secondary electrons; (4) secondary electrons are repelled from cathode walls and become trapped in the bulk plasma; (5) electrons oscillating about the axis of hollow cathode ionize more argon; (6) ionized argon is again accelerated to cathode wall and produces more secondary electrons; (7) positive feedback loop continues building up electron reservoir in hollow cathode; and (8) electron beam is extracted from the hollow cathode.

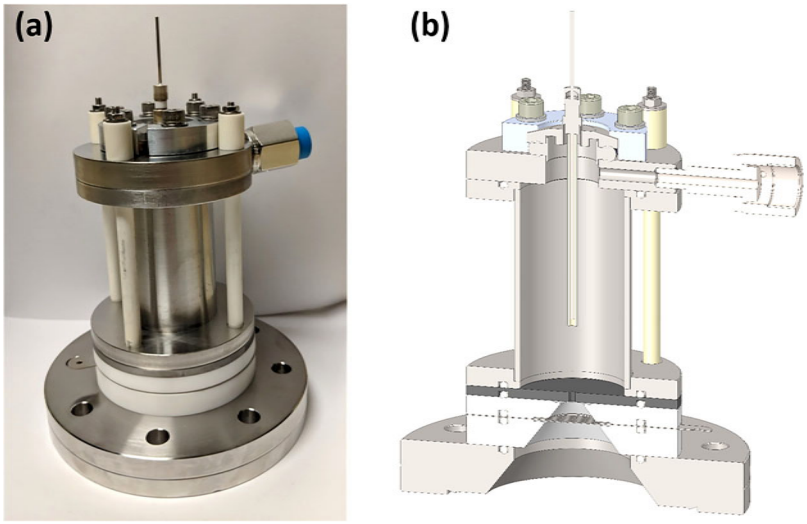

FIG. 2. (a) Picture of assembled HC-PES before installation on the chamber. (b) Cross section of HC-PES.

ionize and excite additional argon atoms before losing most of their kinetic energy. (6) The newly created ions are again accelerated toward the walls, liberating more secondary electrons during their collision with the walls. (7) The secondary electrons, as well as electrons from argon ionization, join the existing electrons in the hollow cathode body, further ionizing more neutral species. This process of ionization, acceleration, secondary electron liberation, electron oscillation, and further ionization continues until reaching a steady state. (8) When the potential of the hollow cathode plasma is sufficiently negative relative to the anode bias, an electron current can be extracted from the hollow cathode plasma.

B. Hollow cathode plasma electron source

Figure 2(a) shows a picture and Fig. 2(b) displays a cross-sectional view of the HC-PES used in this study. This HC-PES was based on an earlier HC-PES design developed at the Naval Research Laboratory.[13,29] The hollow cavity has an inner diameter of 3.5 cm and a length of 6.8 cm. Argon gas flows in at the top of the hollow cavity. The argon gas flows out an aperture at the bottom of the hollow cavity. The aperture also allows electrons to escape from the HC plasma source toward the bias grid. The diameter of the aperture is 1.5 mm.

The geometry is an important aspect of the HC-PES design.[17] In particular, when the aperture area is very small compared with the interior surface area of the hollow cathode, most of the discharge voltage appears across an ion sheath at the cathode wall. The corresponding electron flux required for quasineutrality appears at the anode grid which is positive with respect to the plasma potential. When the ratio of the effective anode surface area (A_a) to cathode surface area (A_c) satisfies $(A_a/A_c) < (m_e/m_i)^{1/2}$, where m_e and m_i are the electron and ion masses, respectively, the electrons leave the plasma source through an electron sheath at the anode, and the electron beam current can ideally be as large as the discharge current.[17,30]

Figure 3 displays a schematic of the HC-PES. The HC-PES operates at an argon gas pressure of approximately 350 mTorr. This Ar pressure is determined using the Ar gas throughput and the estimated gas conductances. The wall of the hollow cavity is the cathode. The cathode is biased at −250 to −350 V relative to the bias grid voltage. The power supply for the HC plasma is referenced to the bias grid, which is biased with respect to the ground.

Electrons extracted from the hollow cathode plasma are then accelerated by the grid bias. The nonambipolar flow conditions established by the geometry produce an electron sheath at the acceleration grid, with a potential that scales with electron temperature.[29] The electron beam energy will be the sum of the electron sheath potential and bias applied to the grid. The electron sheath

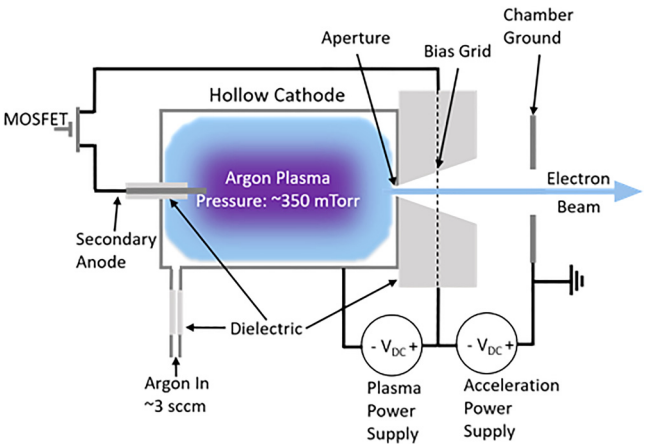

FIG. 3. Schematic of the HC-PES showing the electrical diagram, gas flow and approximate pressures, plasma in the hollow cathode cavity, and emitted electron beam.

potential is not known in this work. Consequently, the beam energy will be reported as the grid bias. The electron sheath potential will typically add an additional 20–40 eV to the grid bias to define the electron energy.[29]

A coaxial secondary anode inside the HC is incorporated to switch the electron beam on and off.[13,29] This coaxial secondary anode is located on top of the HC-PES as shown in Fig. 2. The anode is a thin tungsten filament that can be electrically connected to the bias grid through a MOSFET. When the MOSFET is on, this connection effectively shunts the electrons in the plasma to the secondary anode. When the MOSFET is off, the secondary anode floats to the plasma potential within the cathode and electrons will flow through the aperture to reach the bias grid.

The plasma power supply is current-limited to restrict the heating of the hollow cathode. For the majority of the experiments, the current was limited at 200 mA. The electrons in the emitted beam must be replenished by the power supply. Consequently, the current limit on the plasma power supply also regulated the electron beam current to the sample. Much more current could be extracted if the hollow cathode was allowed to run at higher temperatures. However, the hollow cathode plasma would be harder to control at these higher temperatures.

The sample is connected to the chamber ground. The grounding of the sample prevents the sample from building up a potential that would then deflect incident electrons. The sample current can be quantified by installing an ammeter between the sample and ground. This sample current is a direct measure of the electron current to the sample from the HC-PES. The sample current determines the time required to desorb ligands from the surface during EE-ALD.

C. Electron steering optics

Figure 1 shows that ions are accelerated toward the wall of the hollow cathode. These ions collide with the wall at a kinetic energy of hundreds of electron volts. These collisions produce secondary electrons that sustain the plasma. In addition, these collisions also sputter the walls of the hollow cathode, with a yield that depends on ion energy. While this sputtered material can be used for thin film deposition if the sputtered species have line-of-sight to the substrate,[24] the sputtered material will adversely affect the purity of the films grown by EE-ALD in this study.

In the hollow cathode displayed in Fig. 2, the enclosed nature of the hollow cathode cavity confines most of the sputtered material inside the hollow cathode. However, some of the sputtered material can leave the hollow cathode cavity through the aperture where the electron beam exits. In addition, the aperture can be sputtered by ions in the hollow cathode cavity, where ions hitting the edge of the aperture can lead to forward scattering of sputtered species. Sputtering of the edges of the aperture can enlarge the aperture. This enlargement will eventually affect the pressure differential across the aperture that is necessary to sustain the plasma. The pressure differential is important to maintain a lower pressure in the chamber to provide a long mean free path for the electrons to reach the sample. To minimize this sputter yield, a sputter resistant material can be chosen for the aperture. Molybdenum, tungsten and tantalum have fairly low sputtering yields.[31] For the hollow cathode in this study, molybdenum was used as the aperture material since molybdenum is relatively easy to machine.

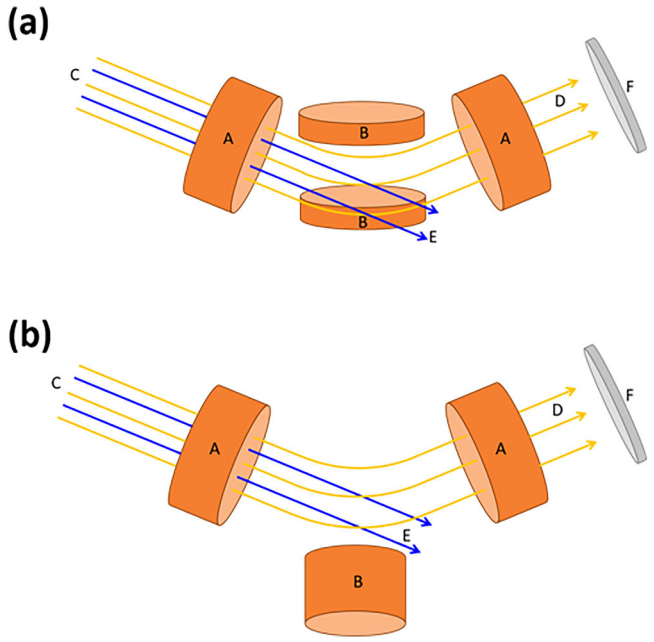

FIG. 4. Schematic of installed electron optics with (a) two steering coils above and below bend and (b) one steering coil outside bend. Schematic designates: (A) collimating coils; (B) steering coil; (C) electron beam with sputtered material from HC-PES; (D) clean electron beam; (E) sputtered material separated from electron beam; and (F) sample.

To address the sputter deposition on the sample, electron optics were developed to steer the electron beam through a bend. The sputtered neutrals are not affected by the electron steering optics and do not pass through the bend, thereby eliminating line-of-sight from the cathode to the sample. Illustrations of the bending of electrons by magnetic fields defined by electromagnetic coils are shown in Fig. 4. Any sputtered ions should be attracted to the negative potential on the cathode wall or bias grid before they enter the electron steering optics. The magnetic fields used in this work were not sufficient to steer any possible ion transmission.

The electron steering optics in Fig. 4(a) were composed of a pair of on-axis collimating electromagnetic coils and a pair of off-axis steering electromagnetic coils above and below the bend. A photograph of these collimating and steering electromagnetic coils is given in Fig. 5(a). The electron beam diverges because electrons repel each other as they travel due to space charge effects. The on-axis coils collimate and center the electron beam. The magnetic field from the collimating coils provides a track for the electrons. The electrons spiral along the field lines, packing more closely as the magnetic field strength increases in the region of the coil.

The off-axis steering coils alone should be able to bend the electron beam and sweep the beam alignment in the plane of the bend. This sweep of the beam alignment provides precise

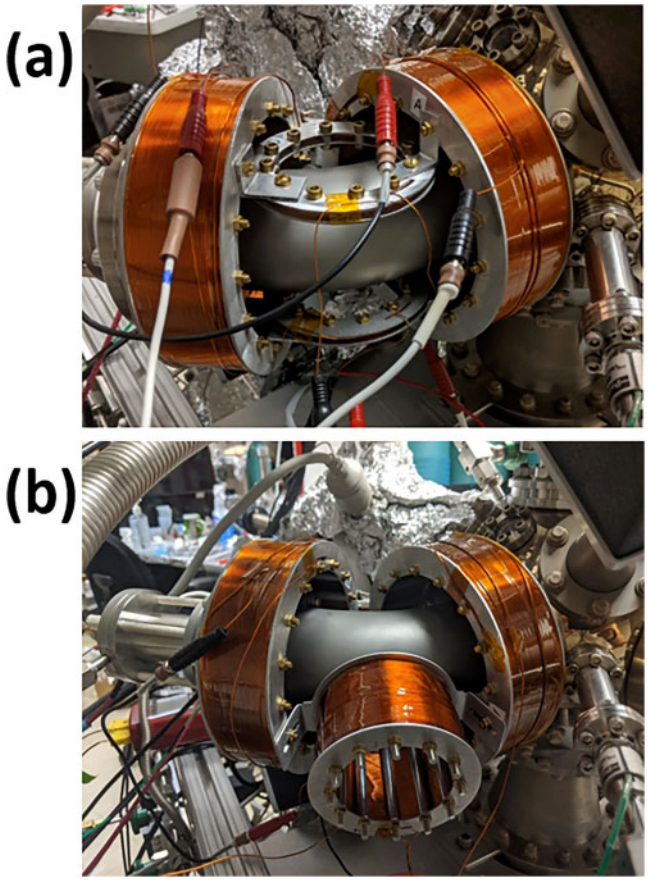

FIG. 5. Picture of installed electron optics with (a) two steering coils above and below the bend and (b) one steering coil outside the bend. HC-PES is to the left of the leftmost collimating electromagnetic coil. The main chamber and the sample are to the right of the rightmost collimating electromagnetic coil.

positioning of the electron beam in the horizontal plane on the sample stage. However, when combined with the large magnetic fields from the on-axis electromagnetic coils, the off-axis coils in Fig. 4(a) were not able to move the electron beam enough to position the electron beam on the exact center of the sample stage.

Determining the electron beam center on the sample stage is difficult when the electron flux is sufficient to remove all ligands from the saturated surface after precursor adsorption. In this electron flux limit, the spatial distribution of the deposited film is uniform. To identify the electron beam center, electron-enhanced BN chemical vapor deposition (CVD) was employed using borazine as the sole-source precursor.[4] BN EE-CVD does not exhibit the self-limiting behavior associated with saturation. Consequently, the spatial deposition of the BN EE-CVD can reveal the electron beam center.

The updated configuration, shown in Fig. 4(b), was implemented for more precise alignment of the electron beam. This configuration has a single off-axis electromagnetic coil positioned outside the bend. This coil effectively pushes the beam around the bend and steers the electron beam. A photograph of the collimating and steering electromagnetic coils corresponding to Fig. 4(b) is given in Fig. 5(b). This configuration results in more accurate positioning of the electron beam at the center of the sample stage than the configuration shown in Figs. 4(a) and 5(a).

Several configurations of electromagnetic coils were used for the different experiments as described in the text. Both configurations shown in Fig. 4 were effective at bending the electron beam and separating the electron beam from the sputter yield. Prior to installing the electron steering optics, *in situ* Auger Electron Spectroscopy (AES) of samples subjected to electron beam exposures showed an Mo AES signal. In contrast, no Mo AES signals were observed after the installation of the electron steering optics.

III. EXPERIMENTAL FOR Co EE-ALD

Co EE-ALD films were grown in a vacuum apparatus chamber that has been described previously.[1,3,4] The main UHV chamber with a base pressure of 2×10^{-9} Torr is equipped with a load lock that allows samples to be introduced without breaking vacuum. The main chamber also contains an *in situ* ellipsometer (Filmsense1) and mass spectrometer (PrismaPlus QMG 220, Pfeiffer Vacuum). In addition, a picoammeter (Keithley) is attached to the sample stage to measure the incident electron current. An analysis chamber containing an *in situ* AES spectrometer (RBD, microCMA) is also attached to the main chamber.

The Co EE-ALD films were grown on Si wafer coupons (Silicon Valley Microelectronics, boron doped). The Si coupons contained the native oxide on the silicon surface. Prior to the insertion into the vacuum apparatus, the Si coupons were washed in methanol and acetone and blown dry with ultrahigh purity nitrogen. The Si coupons were then loaded into the load lock chamber following procedures that have been detailed earlier.[1]

The Co EE-ALD growth was conducted using a pulse sequence consisting of (1) cobalt tricarbonyl nitrosyl [$Co(CO)_3NO$, CTN] adsorption; (2) pump time; (3) electron beam exposure; and (4) pump time before the next CTN adsorption. The timing for this pulsing sequence can be characterized by (t_1, t_2, t_3, t_4). The following is representative of the parameters in a typical experiment. The CTN precursor was kept at 3 Torr behind a micropulse valve. The valve was actuated for $t_1 = 0.5$ s. The valve opening led to a transient pressure in the main chamber of $\approx 5 \times 10^{-3}$ Torr. Pumping was then performed for a total of $t_2 = 20$ s. The electron exposure was then performed with a grid bias of 140 V for $t_3 = 2$ s, with an electron current of >50 mA. The next CTN adsorption was then conducted after a pump time of $t_4 = 20$ s. The timing for this pulsing sequence was (0.5, 20, 2, 20). The sum of these steps produced a reaction cycle time of ≈43 s.

In situ ellipsometry (Filmsense, FS1) measurements were collected every second throughout the deposition. The *in situ* ellipsometer uses four wavelengths of light. The precision of the *in situ* ellipsometry measurements of film thickness is within ± 0.03 Å. *Ex situ* spectroscopic ellipsometry (Model M-2000, J.A. Woollam Co., Inc.) was also performed to measure the film thickness and determine the spatial profile of the deposited film. The data were fit using a B-spline model in CompleteEase (J.A. Woollam Co., Inc.)

with n and k values for Co as a starting point. Focusing probes that reduce the spot size to 0.3–0.4 mm were used for data acquisition.

The technique of *in situ* lift-out in an FEI Nova 600 Dual Beam SEM/FIB was used for preparing cross-sectional TEM specimens. The surfaces of the specimens were polished with a low energy (2 keV) Ga ion beam to minimize the damaged layer caused by focused ion beam (FIB) milling. All HAADF-STEM images and EDS maps were acquired at 300 kV on a spherical aberration corrected FEI Titan Themis equipped with a Bruker Super-X quad EDS detector.

IV. RESULTS AND DISCUSSION

A. HC-PES characterization

The HC-PES can produce an electron beam with high currents. Figure 6 shows the measured sample current versus the HC-PES power supply current. The power supply current can be turned up even higher to produce a proportionally larger sample current. However, these larger power supply currents lead to heating of the hollow cathode. This heating must be contained because of the thermal limits of the Viton O-Rings that are used to seal the various components that define the HC-PES. Constructing an HC-PES without using temperature sensitive materials is possible. The present setup with Viton O-Rings allows easy access to the hollow cathode cavity and replacement of the aperture. Importantly, the electron currents obtained with the present HC-PES are sufficient for EE-ALD experiments to be conducted in a timely manner.

Another advantage of the HC-PES is the rapid on/off switching of the electron beam. Figure 7 shows a comparison between the HC-PES and an electron flood gun (FRA-2 × 1–2, Kimball-Physics Inc.) for obtaining full current to the sample. For the HC-PES, the electron beam can be effectively turned on/off by switching with a MOSFET that provides access to a secondary anode. When the MOSFET is on, most of the electrons flow through the secondary

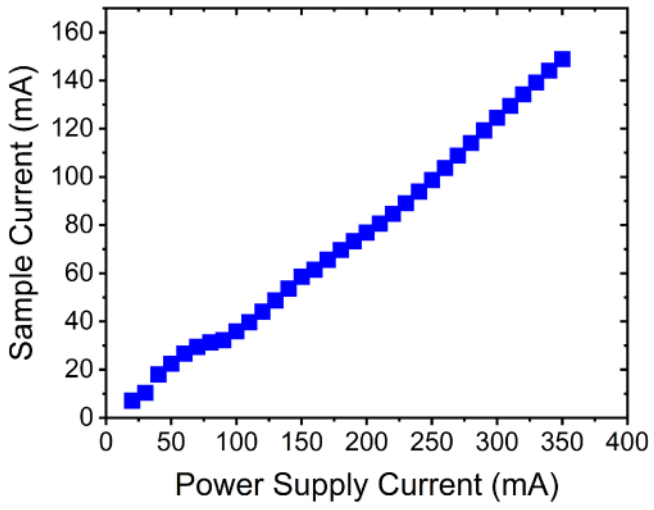

FIG. 6. Sample current as a function of the power supply current.

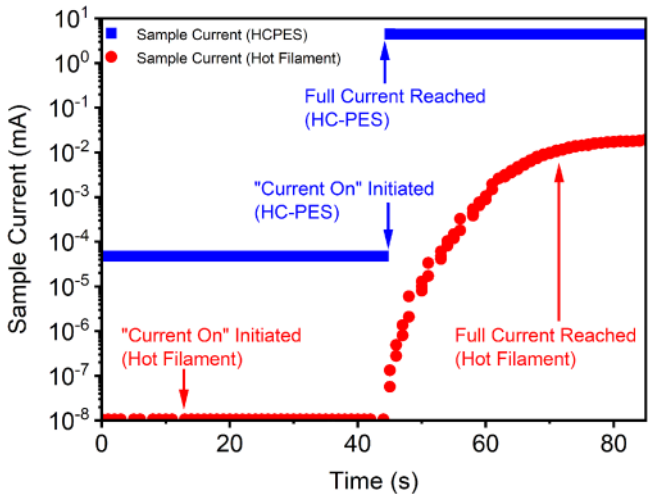

FIG. 7. Comparison of the start-up time of the electron gun and HC-PES. Electron gun reached full current in >1 min. HS-PES reached full current in <10 ms.

anode. Figure 7 indicates that only a small number of electrons can travel through the aperture and reach the sample when the MOSFET is turned on. This "leakage" current from the HC-PES is almost three orders of magnitude less than the full electron current from the electron gun. These low electron currents have a negligible effect on Co EE-ALD.

Upon turning off the MOSFET, the electron beam can exit the aperture at the front of the HC-PES and reach the sample. Figure 7 reveals that the electron beam is reestablished in less than the 10 ms time resolution of the ammeter used to make the measurement.[29] In contrast, Fig. 7 shows that the electron gun used in previous work requires several minutes to obtain an electron beam from the hot filament.

Figure 7 also illustrates the dramatic difference in electron current from the HC-PES and the electron flood gun. Electron currents from the HC-PES described in this publication easily reach 100 mA over a 10 cm^2 area in the steady-state operation. This is a factor of 3000× more current over an area 10× larger than for the previous electron flood gun. The factor of 3000× more current over an area 10× larger is an increase of 300× in the electron flux. The essentially immediate on/off switching and the 300× increase in the electron flux lead to a dramatic reduction in cycle time for EE-ALD.

The chemical insensitivity of the HC-PES is also important in reducing the EE-ALD cycle time. The hot filament in the electron flood gun must not be hot when the precursor is present in the reactor to avoid precursor decomposition on the filament that leads to CVD. This CVD can lead to corrosion of the filament or change its work function. These changes can decrease both filament lifetime and the electron emission from the hot filament. To avoid this CVD, the precursor must be completely removed from the chamber prior to and after heating the filament.

Previous EE-ALD experiments using electron flood guns have reported that the time required for filament warm up, cool down, pumping, and electron exposure with low electron flux can be as long as 15 min for just the electron exposure step.[1–4] In contrast, an EE-ALD cycle using the HC-PES is essentially as long as the electron exposure. Electron exposures are usually on the order of 10 s. Long pump or purge times are not necessary because the HC-PES is chemically insensitive.

B. Co EE-ALD growth characteristics

Co EE-ALD can be performed using sequential exposures of CTN and electrons.[1] The surface reactions during one cycle of Co EE-ALD using CTN and electron exposure are given as follows:

$$\mathrm{Co^{*} + Co(CO)_3NO(g) \rightarrow Co\text{-}Co(CO)_3NO^{*}}, \quad (1)$$

$$\mathrm{Co\text{-}Co(CO)_3NO^{*} + e^{-} \rightarrow Co\text{-}Co^{*} + 3CO(g) + NO(g)}. \quad (2)$$

The asterisks indicate the surface species. Co EE-ALD films are grown by repeating the Co EE-ALD cycles. The desorption of CO and NO during electron exposures has been confirmed earlier using quadrupole mass spectrometry investigations.[1] The cobalt thickness versus spatial position after a number of Co EE-ALD cycles reveals the electron beam on the sample.

A comparison of spatial profiles for Co EE-ALD is shown in Fig. 8. Figure 8(a) displays the spatial profile of the focused electron beam from the hot filament electron gun.[1] The electron gun has a small spot size of approximately 1 cm^2. The electron flux achieves saturation of the ESD reaction as revealed by the "flat top" profile over a small, ≈0.25 cm^2 area of the substrate. Additional calculations confirmed that the "flat top" profile was a signature of saturation behavior.[1]

The electron exposure time required to achieve saturation at the center of the electron beam spatial profile for the cobalt deposition shown in Fig. 8(a) during Co EE-ALD was 16 min with the electron gun.[1] A Co film thickness of ≈289 Å was measured after 198 EE-ALD cycles with an electron energy of 200 eV.[1] The dependence of the Co EE-ALD growth rate on electron energy was examined using electrons from the electron gun.[1] The growth rate was highest at a lower electron energy of 125 eV. For the results in Fig. 8(a), the incident electron current on the sample was 21 μA. The time for one EE-ALD cycle was 21 min. The total processing time was 69.3 h.

In contrast, Fig. 8(b) shows the spatial profile for cobalt deposition after Co EE-ALD using the HC-PES. The constant Co thickness of ≈435 Å indicates that the electron exposures can provide saturation exposures over these surface areas of at least 4 cm^2. There is no "flat top" profile because the film thickness is uniform over the entire substrate. The HC-PES can deposit a more uniform Co film thickness over a larger surface area in much less time than the electron gun. These results were obtained after 156 Co EE-ALD cycles using a grid bias of 140 V at an electron current of 10 mA. Given the time for one EE-ALD cycle of 110 s, the total processing time was 4.8 h. Compared with the electron gun, this performance with the HC-PES represents an order of magnitude increase in area in an order of magnitude less time to produce Co films of comparable thickness.

The spatial profile after cobalt deposition shown in Fig. 8(b) was performed prior to installing the electron steering optics displayed in Fig. 5. For this cobalt deposition, the HC-PES had line-of-sight to the sample, with the electron flux directed along the surface normal. A single electromagnetic coil was also used to

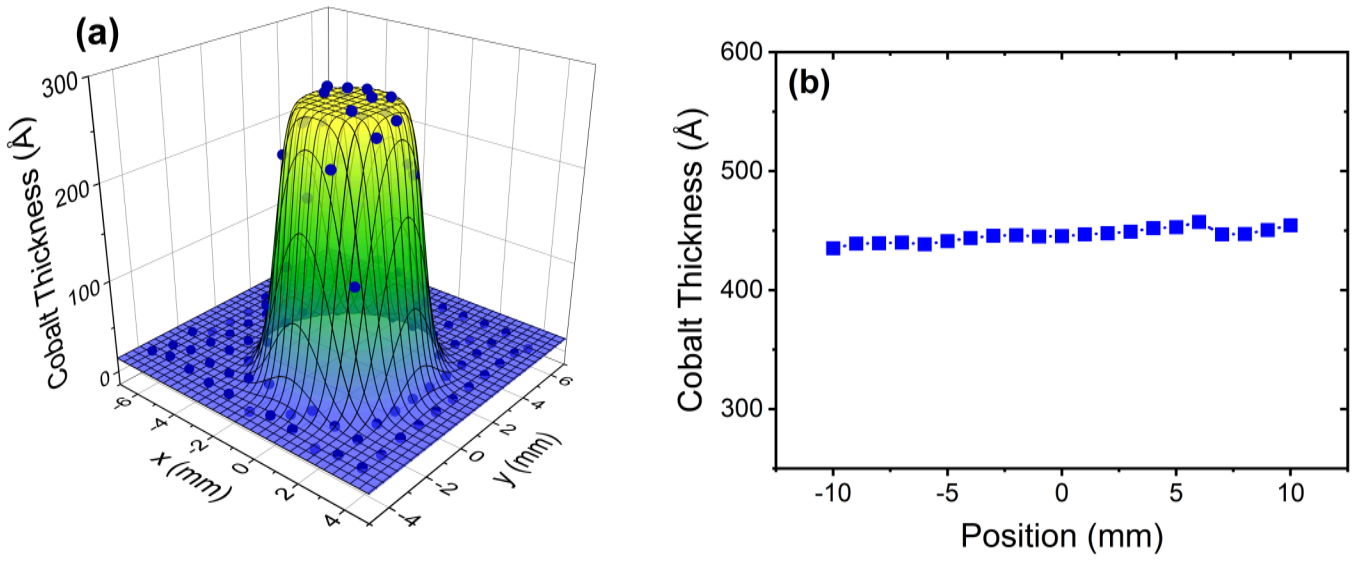

FIG. 8. Comparison of (a) three-dimensional spatial profile of the Co EE-ALD film grown using the electron flood gun and (b) two-dimensional spatial profile of the Co EE-ALD film grown using the HC-PES.

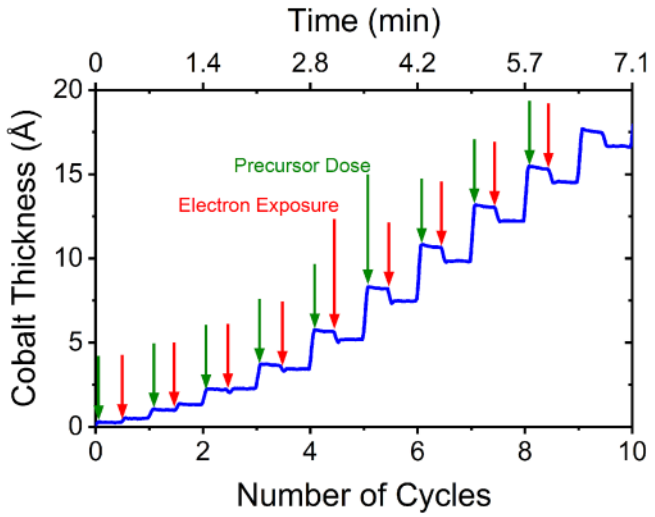

FIG. 9. *In situ* real time ellipsometry of Co EE-ALD nucleation on native oxide on Si coupon. The growth rate at a steady state was 2.4 Å/cycle.

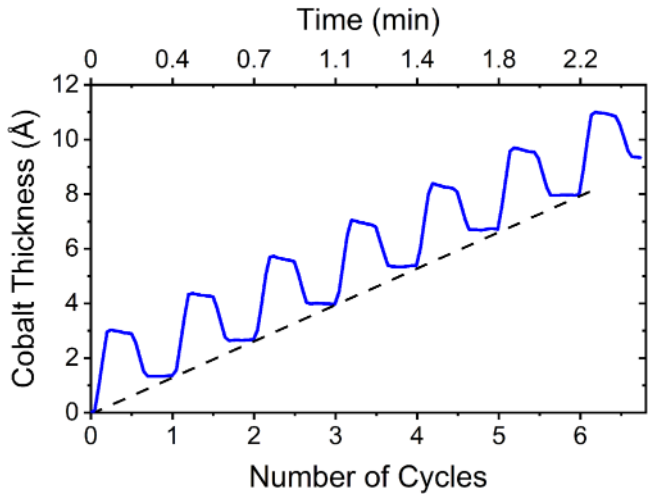

FIG. 11. *In situ* real time ellipsometry of Co EE-ALD on a previously deposited Co film. The Co film growth shows linearity with EE-ALD cycle time of 22 s using short electron exposures of 1.0 s. The growth rate is 1.3 Å/cycle.

collimate the electron beam. The time for one EE-ALD cycle was 110 s. During this EE-ALD cycle, 80 s were dedicated to the electron exposure. The single collimating coil focused fewer electrons onto the sample. This necessitated the longer electron exposure time of 80 s. *In situ* AES measurements determined that the Mo composition in the Co EE-ALD film was 11 at. %. The Mo impurities were eliminated after the installation of the electron optics. Other impurities that remained in the film were C, O, and N at 6.0, 22.6, and 6.2 at. %, respectively.

Figure 9 shows the initial nucleation of Co EE-ALD on the native oxide of the Si coupon using the steering optics shown in Fig. 5(a). The electron current was 72 mA for 1.5 s with a grid bias of 140 V. The pumping time was 20 s before and after each electron exposure. The total cycle time was 43 s. The *in situ* ellipsometry measurements observe deposition from the first electron exposure. The thickness increases with each precursor dose. The measured thickness is then constant until the electron exposure. The electron exposure leads to a reduction of the measured thickness.

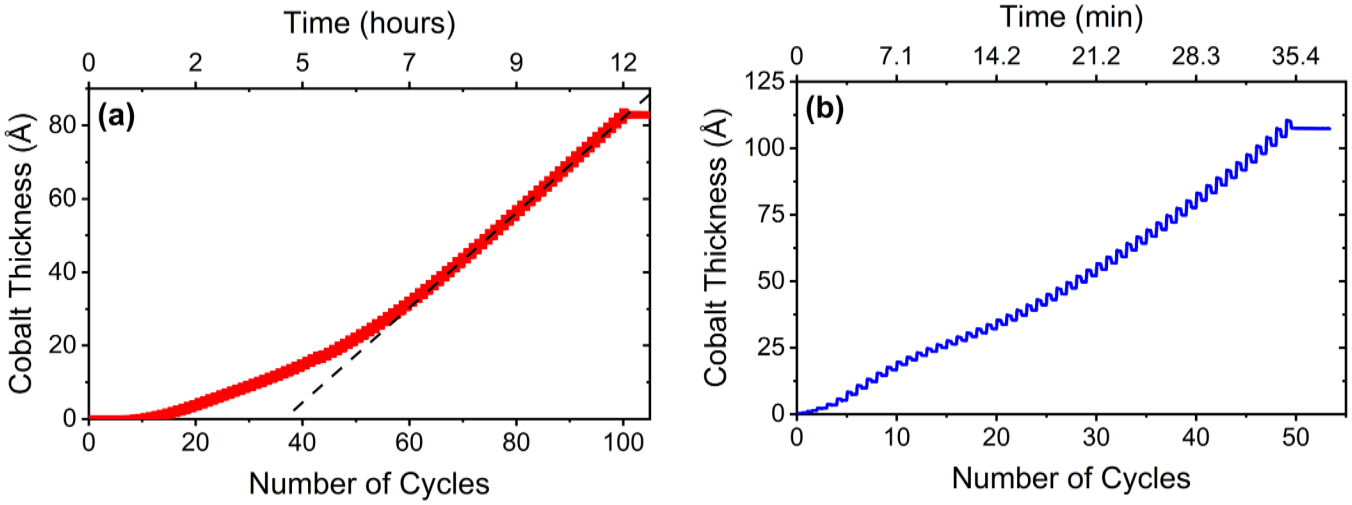

FIG. 10. Nucleation of Co EE-ALD using (a) electron flood gun and (b) HC-PES. Co EE-ALD with the electron flood gun had an EE-ALD cycle time of 7 min and a steady-state growth rate of 1.3 Å per cycle after nucleation. Co EE-ALD with HC-PES had an EE-ALD cycle time of 43 s and a steady-state growth rate of 2.4 Å per cycle after nucleation.

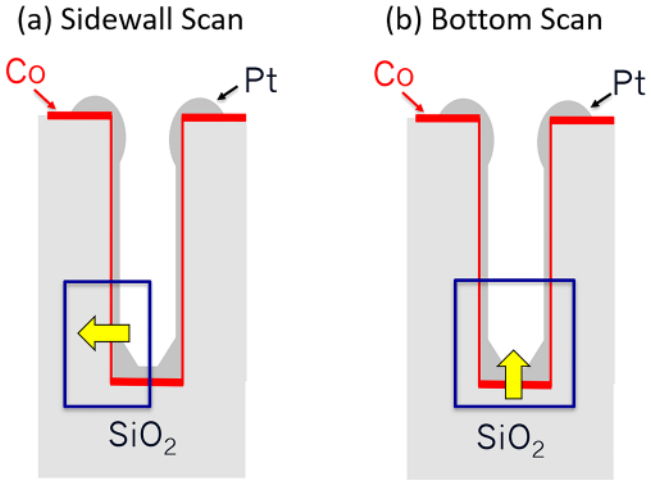

FIG. 12. Schematic showing via locations for (a) sidewall scan and (b) bottom scan.

The Co EE-ALD film nucleates in 4 EE-ALD cycles. The cobalt film growth is then very constant at 2.4 Å/cycle for subsequent EE-ALD cycles.

To appreciate the significance of these results, Fig. 10 compares the nucleation of Co EE-ALD using the electron gun and the HC-PES. The HC-PES obtains much more rapid nucleation of Co EE-ALD than the electron flood gun. In Fig. 10(a), there is a delay of approximately 10 cycles before observing any deposition.[1] Between 10 and 50 cycles, the deposition occurs and increases progressively with the number of cycles. The EE-ALD reaches the steady-state growth after approximately 50 cycles. These results were obtained with an electron energy of 100 eV and an electron current of 21 μA with the electrons focused to a Gaussian spatial profile with a waist of ≈2.5 mm.[1] The EE-ALD cycle time was 7 min.

Extended nucleation times similar to the long nucleation period observed in Fig. 10(a) are typical for metal ALD on metal oxides.[32–34] For EE-ALD, one possible explanation for the long nucleation period is that the low electron fluxes from the electron gun were not adequate to create sufficient active sites on the substrate. Consequently, many EE-ALD cycles were required for enough nucleation sites to build up on the surface and eventually lead to linear growth.

In contrast, nucleation is much more rapid during Co EE-ALD using the HC-PES. Figure 10(b) shows the rapid nucleation of Co EE-ALD. These results are an extension of the results described above and depicted in Fig. 9. Cobalt deposition is observed during the first EE-ALD cycle. The Co deposition increases progressively between the 2nd and 6th EE-ALD cycles. Subsequently, the Co EE-ALD film proceeds to grow linearly with a growth rate of 2.4 Å/cycle. These results were obtained with a grid bias of 140 V and an electron current of 72 mA for an electron exposure time of 1.5 s with the electrons illuminating an area of at least 2 × 2 cm^2. The EE-ALD cycle time was 43 s.

The Co EE-ALD film growth with the HC-PES was observed to be linear over a wide range of electron exposures. The large electron flux of the HC-PES allows electron exposures to be short and still achieve growth rates >1 Å per EE-ALD cycle. Figure 11 shows results for the cobalt thickness versus the number of cycles for shorter electron exposure times of 1 s. The growth rate is 1.3 Å per EE-ALD cycle with the electron exposure time of 1 s. These results were obtained with a grid bias of 140 V and an electron current of 65 mA with the electrons illuminating an area of at least 4 cm^2 using the electron steering optics shown in Fig. 5(a). The EE-ALD cycle time was 22 s with pumping times of 10 s before and after each electron exposure.

The interpretation of these results in Fig. 11 is that the shorter electron exposure times of 1 s at 65 mA from the HC-PES desorb fewer ligands from the surface than the longer electron exposure times of 1.5 s at 72 mA. The ligands left behind after the smaller electron exposure lead to lower precursor adsorption during the

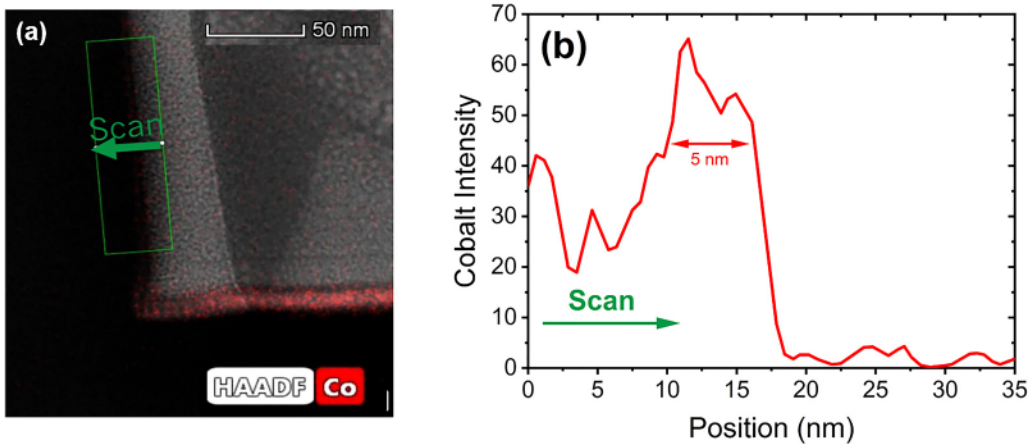

FIG. 13. (a) TEM image of via showing the location of the sidewall scan and (b) the EDS line scan for Co on the vertical sidewall yielding a Co film thickness of ≈5 nm.

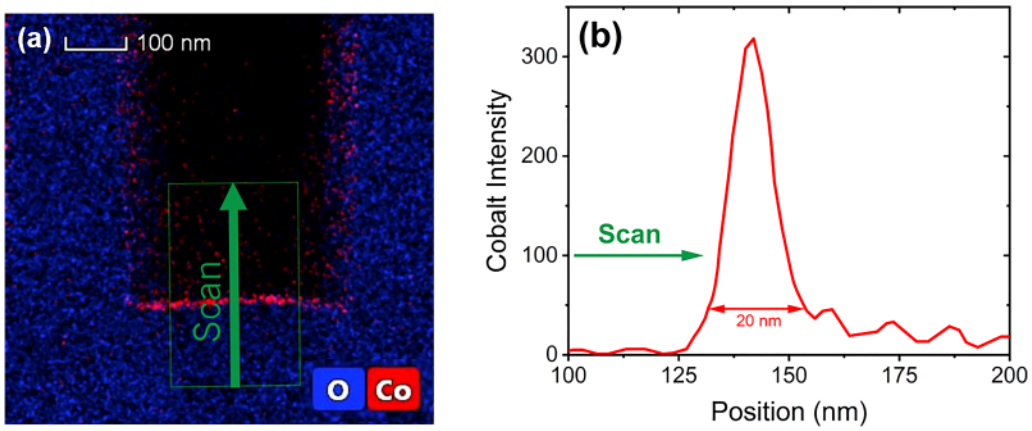

FIG. 14. (a) TEM image of via showing the location of the bottom scan and (b) the EDS line scan for Co on the horizontal bottom yielding a Co film thickness of ≈20 nm.

next EE-ALD cycle. The lower precursor adsorption leads to the lower observed growth rates. The linearity of the EE-ALD growth can be attributed to the consistency of the electron exposure during each EE-ALD cycle. As long as the electron desorption is repeatable, linear EE-ALD growth is possible with smaller electron exposures.

One advantage of EE-ALD is the ability to deliver a directed flux of electrons to the surface. To explore the effect of this directed flux, the HC-PES was used for Co EE-ALD on patterned substrates. The pattern consisted of vias with vertical walls, oriented parallel to the surface normal. The vias were approximately 200 nm wide and approximately 1000 nm deep. The Co EE-ALD was performed prior to installing the electron steering optics. The HC-PES was line-of-sight to the sample with the electron flux along the surface normal. A single electromagnetic coil was used to collimate the electron beam.

The Co EE-ALD on patterned substrates was performed with an expected growth rate of 2.4 Å/cycle. The Co EE-ALD was conducted with a grid bias of 140 V and an electron exposure of 10 mA for 80 s. Based on various *in situ* AES studies, the Mo composition in the Co EE-ALD film could have been as much as 15 at. %. This Mo inclusion coupled with *ex situ* air oxidation may account for the large deposition thickness as measured by TEM.

Figure 12 shows a representation of the TEM and energy dispersion (EDS) scans on the sidewall and bottom of the via after Co EE-ALD on the patterned substrates. The actual TEM and EDS line scans for the sidewall and bottom of the via are displayed in Figs. 13 and 14, respectively. The boxes in Fig. 12 identify the areas of the via that are scanned in Figs. 13 and 14.

The topographical area selectivity of the Co EE-ALD is apparent from an examination of the Co line scans in Figs. 13 and 14. The EDS line scan on the sidewall of the via in Fig. 13(b) reveals that the Co EE-ALD has a thickness of approximately 5 nm. This thickness is probably larger than the actual thickness because the vias have a curved surface. Scans across this curved surface detect signal from the surface area that is not in the same plane as the focused ion beam cut required for imaging.

In comparison, the EDS line scan on the bottom of the via in Fig. 14(b) reveals that the Co EE-ALD has a thickness of approximately 20 nm. In this case, the width of the Co thickness is more precise because there is no Co EE-ALD beyond the bottom of the via. A comparison of the ≈5 nm thickness on the sidewall of the via and the ≈20 nm thickness on the bottom of the via yields a topographical selectivity of 4:1.

This topographical area selectivity of 4:1 in favor of horizontal surfaces is expected given the direction of the electron flux. More of the electron flux oriented along the surface normal is incident on horizontal surfaces. The vertical sidewalls are parallel to the electron flux. ESD from the vertical sidewalls will occur resulting from electron beam misalignment, electron deflection due to charging, or electron scattering in the vias. This topographical area selectivity may allow Co EE-ALD to achieve bottom-up fill of trenches and vias.

V. CONCLUSIONS

A HC-PES was built and utilized for EE-ALD. The HC-PES produced high electron currents >200 mA that could be turned on/off in <10 ms. These higher electron fluxes and much smaller purge times facilitated by the chemical robustness of the HC-PES led to short EE-ALD cycle times. This performance was greatly improved compared with the electron currents and cycle times from a previous electron flood gun source. The total process times using the HC-PES decreased by as much as an order of magnitude or more compared with the electron gun source. The sputter yield from the HC-PES was eliminated using electron steering optics defined by electromagnetic coils.

The higher electron flux from the HC-PES led to very uniform Co thin films using sequential exposures of $Co(CO)_3NO$ and low energy (100–200 eV) electrons. The Co films were uniform over the entire surface area of ≈4 cm^2, suggesting that the electron exposures were sufficient for the ESD of surface species to reach saturation. The high electron fluxes also led to the rapid nucleation of Co EE-ALD films on the native oxide on Si coupons. The Co EE-ALD

films nucleated in as few as four EE-ALD cycles. Steady-state Co growth rates of >2 Å/cycle were observed over the entire surface area. Shorter electron exposures also led to linear film growth at slightly lower growth rates.

TEM and EDS was used to analyze Co EE-ALD on high aspect ratio features. Co EE-ALD on vertical vias with a width of ≈200 nm and a depth of ≈1000 nm displayed a topographical area selectivity. There was a 4:1 topographical selectivity in favor of horizontal surfaces. This topographical selectivity was explained by the directional electron flux incident on the surface normal and parallel to the vertical sidewalls of the vias. This topographical area selective deposition may be useful for the bottom-up fill of trenches and vias.

ACKNOWLEDGMENTS

This work was supported by the Joint University Microelectronics Program (JUMP) funded by the Semiconductor Research Corporation (SRC). This work was also partially supported by the Naval Research Laboratory base program. The authors thank Kenneth Smith and Don David from the University of Colorado Integrated Instrument Development Facility for their construction of the HC-PES and computer interfacing. The authors also thank Dr. Sadegh Yazdi for the TEM sample preparation and high-resolution STEM and STEM-EDS mapping and analysis. The authors acknowledge the support from the Facility for Electron Microscopy of Materials at the University of Colorado at Boulder (CU FEMM). The authors also acknowledge Woodruff Scientific for the modeling and construction of the electron steering optics.

DATA AVAILABILITY

The data that support the findings of this study are available within the article.

REFERENCES

[1]Z. C. Sobell, A. S. Cavanagh, and S. M. George, J. Vac. Sci. Technol. A **37**, 060906 (2019).
[2]J. K. Sprenger, A. S. Cavanagh, H. Sun, K. J. Wahl, A. Roshko, and S. M. George, Chem. Mater. **28**, 5282 (2016).
[3]J. K. Sprenger, H. Sun, A. S. Cavanagh, and S. M. George, J. Vac. Sci. Technol. A **36**, 01A118 (2018).
[4]J. K. Sprenger, H. X. Sun, A. S. Cavanagh, A. Roshko, P. T. Blanchard, and S. M. George, J. Phys. Chem. C **122**, 9455 (2018).
[5]P. J. Feibelman and M. L. Knotek, Phys. Rev. B **18**, 6531 (1978).
[6]M. L. Knotek and P. J. Feibelman, Phys. Rev. Lett. **40**, 964 (1978).
[7]S. M. George, Chem. Rev. **110**, 111 (2010).
[8]K. E. J. Goh, S. Chen, H. Xu, J. Ballard, J. N. Randall, and J. R. Von Ehr, Appl. Phys. Lett. **98**, 163102 (2011).
[9]J. H. G. Owen, J. Ballard, J. N. Randall, J. Alexander, and J. R. Von Ehr, J. Vac. Sci. Technol. B **29**, 06f201 (2011).
[10]Y. Feng and J. P. Verboncoeur, Phys. Plasmas **13**, 073105 (2006).
[11]Y. Y. Lau, Y. F. Liu, and R. K. Parker, Phys. Plasmas **1**, 2082 (1994).
[12]J. R. Bayless, R. C. Knechtli, and G. N. Mercer, IEEE J. Quantum Electron., **10**, 213 (1974).
[13]C. D. Cothran, D. R. Boris, C. S. Compton, E. M. Tejero, R. F. Fernsler, W. E. Amatucci, and S. G. Walton, Surf. Coat. Technol. **267**, 111 (2015).
[14]G. Stockhausen and M. Kock, J. Phys. D: Appl. Phys. **34**, 1683 (2001).
[15]E. M. Oks, Plasma Sources Sci. Technol. **1**, 249 (1992).
[16]E. M. Oks and P. M. Schanin, Phys. Plasmas **6**, 1649 (1999).
[17]E. Oks, *Plasma Cathode Electron Sources: Physics, Technology, Applications* (Wiley-VCH, Weinheim, 2006).
[18]V. Burdovitsin and E. Oks, Rev. Sci. Instrum. **70**, 2975 (1999).
[19]V. A. Burdovitsin and E. M. Oks, Laser Part. Beams **26**, 619 (2008).
[20]V. A. Burdovitsin, I. S. Zhirkov, E. M. Oks, I. V. Osipov, and M. V. Fedorov, Instrum. Exp. Tech. **48**, 761 (2005).
[21]A. Klimov, I. Bakeev, E. Oks, and A. Zenin, Laser Part. Beams **37**, 203 (2019).
[22]V. G. Shchukin, V. O. Konstantinov, and V. S. Morozov, Tech. Phys. **63**, 888 (2018).
[23]I. Osipov and N. Rempe, Rev. Sci. Instrum. **71**, 1638 (2000).
[24]S. Muhl and A. Perez, Thin Solid Films **579**, 174 (2015).
[25]S. G. Walton, D. R. Boris, S. C. Hernández, E. H. Lock, T. B. Petrova, G. M. Petrov, and R. F. Fernsler, ECS J. Solid State Sci. Technol. **4**, N5033 (2015).
[26]S. G. Walton *et al.*, Microelectron. Eng. **168**, 89 (2017).
[27]C. Li, V. Godyak, T. Hofmann, K. Edinger, and G. S. Oehrlein, J. Vac. Sci. Technol. A **38**, 033001 (2020).
[28]L. Bardos, Surf. Coat. Technol. **86–87**, 648 (1996).
[29]D. R. Boris, C. D. Cothran, C. S. Compton, W. E. Amatucci, and S. G. Walton, IEEE Trans. Plasma Sci. **44**, 761 (2016).
[30]S. D. Baalrud, N. Hershkowitz, and B. Longmier, Phys. Plasmas **14**, 042109 (2007).
[31]N. Laegreid and G. K. Wehner, J. Appl. Phys. **32**, 365 (1961).
[32]L. Baker, A. S. Cavanagh, D. Seghete, S. M. George, A. J. M. Mackus, W. M. M. Kessels, Z. Y. Liu, and F. T. Wagner, J. Appl. Phys. **109**, 084333 (2011).
[33]J. W. Elam, A. Zinovev, C. Y. Han, H. H. Wang, U. Welp, J. N. Hryn, and M. J. Pellin, Thin Solid Films **515**, 1664 (2006).
[34]J. Hamalainen, M. Ritala, and M. Leskela, Chem. Mater. **26**, 786 (2014).